

## Article

# Trigno River Mouth Evolution via Littoral Drift Rose

Margherita Carmen Ciccaglione <sup>1,\*</sup>, Mariano Buccino <sup>1</sup>, Gianluigi Di Paola <sup>2</sup> , Sara Tuozzo <sup>1</sup> and Mario Calabrese <sup>1</sup>

<sup>1</sup> Department of Civil and Environmental Engineering, University of Naples Federico II, Via Claudio, 21, 80125 Naples, Italy; buccino@unina.it (M.B.); sara.tuozzo@unina.it (S.T.); mario.calabrese@unina.it (M.C.)

<sup>2</sup> Department of Biological, Geological and Environmental Sciences, University of Bologna, Via Zamboni, 33, 40126 Bologna, Italy; gianluigi.dipaola@unibo.it

\* Correspondence: margheritacarmen.ciccaglione@unina.it

**Abstract:** A mid-term analysis of shoreline evolution was carried out in the present paper for the Trigno river mouth area (5.2 km), located in the northern part of the Molise coast region (southeast Italy). The littoral drift rose (LDR) concept was employed, coupled to the GENESIS one-line model, to produce numerical simulations. The LDR graph was used to define a single, time-invariant, “equivalent wave” component (EW), which was supposed to entirely rule the shoreline changes. Given the inherent bimodality affecting the Molise wave climate, EW could result not significant in forecasting shoreline evolution, since both a climate inversion and a time-varying diffusion extra effect are expected. These aspects, never investigated in the literature, are deepened in the present paper, with the main aims of firstly assessing the explanatory power of the LDR equivalent wave and its significance within a bimodal climate, and secondly checking the role of a time-varying diffusivity. Results confirmed the reliability of the EW concept, even within a bimodal climate. Moreover, the possible effect of a time-varying diffusion, which is expected with a large directional variability, produced insignificant results with respect to the EW.



**Citation:** Ciccaglione, M.C.; Buccino, M.; Di Paola, G.; Tuozzo, S.; Calabrese, M. Trigno River Mouth Evolution via Littoral Drift Rose. *Water* **2021**, *13*, 2995. <https://doi.org/10.3390/w13212995>

Academic Editor: Maria Mimikou

Received: 8 September 2021

Accepted: 19 October 2021

Published: 23 October 2021

**Publisher’s Note:** MDPI stays neutral with regard to jurisdictional claims in published maps and institutional affiliations.



**Copyright:** © 2021 by the authors. Licensee MDPI, Basel, Switzerland. This article is an open access article distributed under the terms and conditions of the Creative Commons Attribution (CC BY) license (<https://creativecommons.org/licenses/by/4.0/>).

**Keywords:** beach processes; shoreline erosion; littoral drift rose; coastal morphodynamics; shoreline diffusion

## 1. Introduction

Analysis and predictions of shoreline variation constitute an essential instrument for integrated coastal zone management. At present, it is observed that many coasts around the world are affected by a deficit of sand, which generates, in most cases, a gradual or fast coastline retreat; of course, this represents a leading concern to coastal scientists and planners.

In this regard, shoreline change can be assessed on different timescales. On the one hand, short-term erosion (hours and days) is accountable for the cumulative damage by a storm, while, on the other hand, the long-term shoreline evolution is rather forced by continuous erosion (or accretion) over months and years. As well explained by [1], in a long-term shoreline change analysis, the assumption of a clear shoreline trend is needed at the considered timescale. In this way, the “steady part” of the beach change signal is primarily controlled by both waves producing long-shore sediment transport and boundary conditions (such as structures). Cyclical and random events, such as storms or seasonal variations in waves, only produce a “noise component”, which overlaps with the steady signal. Consequently, within a long-term analysis of shoreline change, effects due to cyclical phenomena are assumed to cancel over years, while the long-term shoreline trend is led by the spatial variations in the long-shore sediment transport rate. According to practical coastal engineering, the latter is essentially due to the dominant direction of wave climate, commonly well represented by a single wave component, equivalent to the whole climate in terms of littoral transport.

In this regard, among several techniques developed to evaluate the long-shore sediment transport rate, the littoral drift rose (LDR) concept [2,3] represents a potentially useful

tool in order to examine shoreline evolution. In particular, a major finding concerning the LDR concept is that the net littoral drift due to a deep water climate, coming from different directions (Total-LDR), can be reduced into a form (Equivalent-LDR) that is representative of a single equivalent wave component (EW) propagating from a single direction. It is worth highlighting that a suitable approximation of the Equivalent-LDR to the total one is reached when Total-LDR exhibits nearly symmetrical lobes. This occurs whenever the wave climate is coming from a restricted angle. On the contrary, when in a wider wave sector, with two or more directional modes, a poorer fit is obtained, due to the asymmetrically shaped Total-LDR. Since a direct relationship between the concepts of equivalent wave and “shoreline diffusivity” exists, the poor approximation of the Total-LDR to the equivalent one was found to be interpreted by the shoreline diffusion concept, and the peculiar case of a bimodal wave climate affecting a stretch of coast was investigated. In fact, while for restricted wave sectors the shore diffusivity can be considered constant over time, in a bimodal wave climate, the deviation detected between total and equivalent LDR, due to its asymmetrical shape, would suggest a time-varying diffusivity extra effect on shoreline evolution. This aspect, never investigated in the literature, could represent a limitation in forecast shoreline evolution techniques based on the EW concept, since the LDR equivalent wave is not able to account for a varying diffusivity, but only for a constant one.

The results presented below apply to the Trigno river mouth area (5.2 km), located in the northern part of the Molise coast region. In this paper, the Molise case study represents a paradigmatic example due to its exposition to the bimodal climate of the Adriatic Sea. In fact, after presenting the mid-term analysis for the site of interest and reconstructing the Molise LDR graph, a numerical study was carried out using the one-contour line model GENESIS, [1] in order to (1) assess the explanatory power of the LDR equivalent wave and its significance within a bimodal climate, and (2) check the effect of a time-varying diffusivity upon the shoreline response. The first aim was examined by inputting in the GENESIS model an “annual scanned” time series built from the EW of Molise coast, while the second was achieved by implementing two different time-resolute wave climates: the “monthly LDR-equivalent wave climate” and the “frequency-equivalent wave climate”.

## 2. Regional Setting

### 2.1. Molise Coast and Shoreline General Trend

The 36 km long Molise coast faces the Adriatic Sea and lies between the Formale del Molino stream to the north and the Saccione stream to the south (Figure 1). It consists of mostly sandy beaches, except for the rocky cliff of Termoli. Additionally, the Molise region is crossed by many rivers flowing into the Adriatic Sea, among which the Trigno and Biferno are the most important in terms of sediment supply.

The Molise coast has been suffering from severe erosion since the 1950s, principally due to the restrictions imposed to the river flows and the consequent decrease in sediment delivery to the coast [4,5]. Erosive processes due to Molise’s traverses and check-dams were intensively deepened in recent studies [6,7], even in other sites of southern Italy [8]. The progressive erosion process has been dealt with, over the years, using structural measures, which consequently resulted in a “hardening” of the coast (with detached breakwaters and groins) of about 62% [4,9].

A remarkable analysis of Molise coastline evolution has been extensively performed in the last decades. More recently, [10] analyzed the average rate of shoreline change of the entire Molise coast within the reference time interval 2004–2016, using the linear regression rate (LRR) as an indicator. The 2004–2016 shoreline data came from the digitalization in the ArcGis Environment of photograph reliefs from different sources. Specifically, since the digitalization procedure produced a certain degree of uncertainty related to measurement errors of the shorelines, a significance analysis was carried out by [10] for the LRR function of the Molise coast, as briefly summarized below for the sake of clarity.

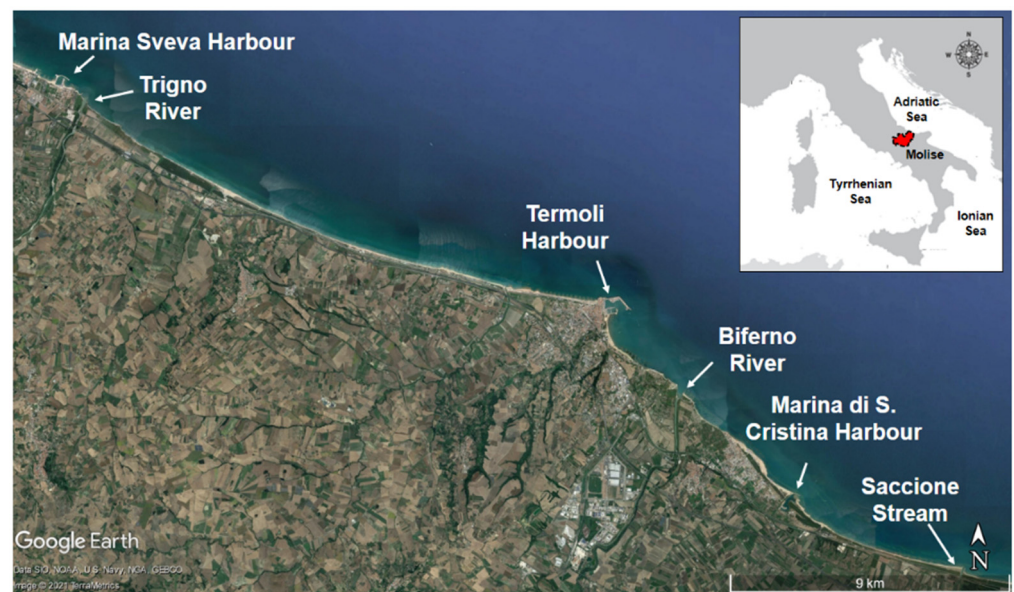


**Figure 1.** Detail of Molise coast.

Treating measurement uncertainties in the frame of the classical theory of errors, the measured shoreline position is seen as the sum of the “true” position plus a random error component, modeled as a Gaussian random variable with zero mean and a standard deviation equal to the root-mean-square (*RMS*) error [10]. Accordingly, the significant *LRR* ( $x$ ) function of the Molise coast was obtained, recognizing areas affected by significant accretion or erosion as those segments of coast where the shoreline change rate exceeds a certain limit value ( $v_{LIM}$ ) and remains above it for a minimum length,  $l_{LIM}$ . The latter was fixed to 500 m, whereas  $v_{LIM}$  [10] was associated with the aforementioned uncertainties of the shoreline measurement process, adopting the linear regression theory [11]. In fact, given the error Gaussianity, the difference between two shoreline measurements at different times is also a Gaussian variable, with zero mean and variance equal to the sum of the squared *RMS* values. Consequently, since the 95% probability level in which the error is included is  $\pm 1.96$ , the root square of the variance, it is possible to calculate the “fictional shoreline rate of change” generated by measurement errors, which is included in the following interval:

$$v_{E95} \cong \pm 1.96 \cdot \frac{\sqrt{RMS_2^2 + RMS_1^2}}{t_2 - t_1}, \quad (1)$$

assuming that the “true” shoreline position remains unvaried in the interval  $t_2 - t_1$ . Therefore,  $v_{LIM}$  is reasonably equated to  $v_{E95}$ , and the  $v_{LIM}$  value detected by [10] for the 2004–2016 time interval was equal to 0.37 m/year, which represents the expected error given by the shoreline surveys.

From the inspection of the *LRR* function of the entire Molise coast, it is possible to recognize that a dominant drift in the north–south direction exists, and that the foremost erosion areas are located south at the Trigno and Biferno rivers. The numerical analysis carried out in the present paper focuses on the Trigno erosion spot, for which a more accurate description is presented in the next section.

## 2.2. Trigno River Mouth

The focus of this article was on a stretch of coast extending from the groin armoring the Trigno river southside mouth, up to 5.2 km southward (Figure 2), which encompasses the sandy beaches of *Costa Verde* and *Marinelle*. In the first 2 km, the reach is defended by a system of 11 groins, with an average length of 68 m and a mean spacing of 170 m.



**Figure 2.** The study area (from A to B, 5.2 km) located just south of the mouth of the Trigno river. The northern part is covered by an 11-groin field.

The analyses of the most recent evolution trends of the Molise coast [4,9,10] all indicated this area as subject to intense erosion, with local rates of retreat as large as  $-8$  m/year. However, the Trigno river mouth and the nearby shoreline have been experiencing significant evolution for nearly 150 years, as well documented in the literature [12].

Halfway through the 20th century, the deltaic mouth system was completely scrapped, consequently moving toward a wave-dominated morphology. In this period, while the delta was eroding, sediment redistribution nourished adjacent beaches, which accreted accordingly. This trend continued until human interventions modified the natural feeding to the shore, thus triggering an erosive process starting from the mid-1950s.

In particular, the S. Salvo check-dam, built about 10 km far from the coast (1954–1977), produced channel tightening over time, leading to a significant sediment volume reduction of the coastal budget [13]. In fact, upstream of the San Salvo check-dam, the channel lowered by ca. 1.5 m during the period 1954–2007 [14]. Conversely, downstream of the check-dam, channel lowering was much greater; from 1954 to 1986, it reached ca. 6.0 m, and, from 1986 to 2007, a further very intense channel lowering of ca. 4.5 m occurred [14]. The significant differences in channel lowering rates between the two stream portions show that the check-dam structure significantly limited river incision upstream. However, since the collapse of the bridge during the flood event in January 2003 [12], the upstream portion started to experience progressive channel incision, now directly affecting the clayey bedrock.

The ongoing erosion has been faced over years with the use of hard structures transverse to the shore; the Trigno mouth was armored around 1980, while the eleven groins southward were built in 1998.

Table 1 reports the shoreline change rate, averaged along the entire reference reach, for either 30 year or 12 year time windows; according to [15], both timeframes can be categorized as “mid-term” intervals.

**Table 1.** Shoreline change rate, averaged along the Trigno river mouth stretch of coast, for either 30 year or 12 year time windows.

Time Window	Average Shoreline Change (m/Year)
1954–1986	−1.52
1986–2016	−2.02
1986–1998	−0.61
1998–2011	−1.94
2004–2016	−2.33

Inspection of the data reveals an increase in the erosive trend over the last 30 years; after the placement of the groin system (1998), the average rate of retreat was on the order of  $-2$  m/year and has seemingly further accelerated in the most recent times (1998–2011 vs. 2004–2016).

The linear regression rate function ( $LRR$ ) for the period 2004–2016 is shown in Figure 3. In the groin-protected area, the average erosion speed is equal to  $-0.94$  m/year, while it exceeds  $-8$  m/year southward. This of course confirms the existence of a prevailing NE to SW littoral drift component, as widely discussed in previous research [4,9,10]. Importantly, referencing the  $x$ -alongshore axis with respect to the 36 km of Molise coast,  $LRR$  is seen to vanish at both  $x = 1760$  m (corresponding to the hydraulic right side of Trigno mouth) and  $x = 6960$  m (red arrows in Figure 3), indicating a negligible rate of evolution, on average, over the period 2004–2016.

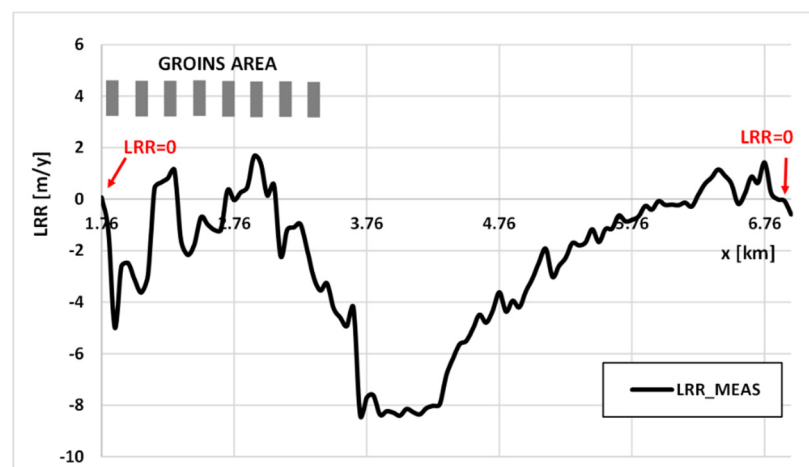


**Figure 3.** Linear regression rate ( $LRR$ ) function of the Trigno river mouth area during the period 2004–2016. The vertical dashes indicate groins; red arrows indicate the  $LRR = 0$  boundary condition.

### 3. Materials and Methods

#### 3.1. Littoral Drift Rose Concept and Shore Diffusivity

The littoral drift rose (LDR) concept, originally introduced by [2,3], represents a powerful help to analyze the long-term shoreline trend. It is a polar representation of littoral transport potential for various shoreline orientations, calculated for a coastal area affected by a uniform deep water wave climate. The latter can be represented by a series of  $N$  wave components,  $(H_{s0,i}; T_{p0,i}; \alpha_{0i})$   $i = 1, \dots, N$ , where  $H_{s0}$  denotes significant wave height,  $T_{p0}$  is the peak period, and  $\alpha_0$  is the azimuth from which waves originate. Furthermore, considering a probability of occurrence,  $p_i$ , for each wave component, the net potential littoral drift rate,  $Q(\beta)$ , for a stretch of coast with normal azimuth  $\beta$ , can be calculated as follows:

$$Q(\beta) = \sum_{\alpha_{0i}=\beta+\frac{\pi}{2}}^{\alpha_{0i}=\beta-\frac{\pi}{2}} p_i \cdot \frac{K \cdot (H_{s0,i})^{2.4} \cdot (T_{p0,i})^{0.2} \cdot g^{0.6}}{16 \cdot (s-1) \cdot (1-n) \cdot \pi^{0.2} \cdot \gamma^{0.4} \cdot 2^{1.4}} \sin[2(\beta - \alpha_{0i})], \quad (2)$$

where  $K$  is a sediment transport coefficient estimated empirically ([16] recommends a value of  $K$  equal to 0.39, based on computations utilizing the significant wave height, while the value of  $K$  corresponding to the root-mean-square wave height is 0.92),  $g$  is gravity,  $s \approx 2.6$  is the ratio between the specific gravity of sediment and that of water,  $n \approx 0.4$  is the in-place porosity, and  $\gamma \approx 0.6$  is the breaker index (wave height to depth ratio).

Equation (2) is based on the well-known CERC formula for littoral drift [16], from which, for each possible shoreline orientation, the annual (or monthly) littoral drifts (positive and negative) are calculated (Figure 4). Particularly, for a certain shoreline orientation  $\beta$ , the LDR graph shows a “node” (Figure 4), where the positive and negative annual-

averaged littoral transports attain the same magnitude and frequency, thus canceling the net transport.

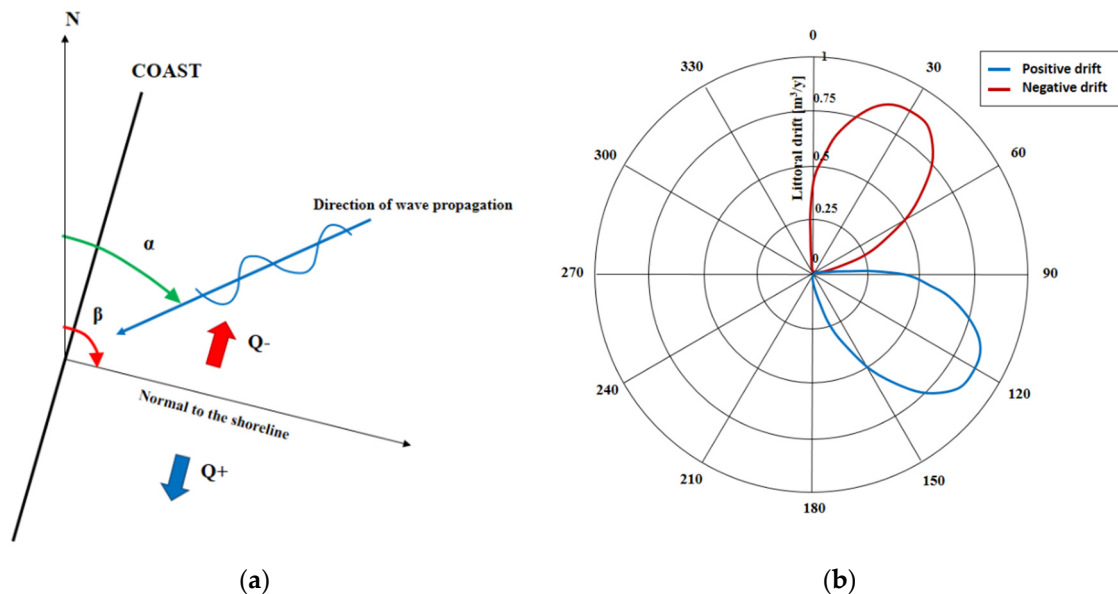


**Figure 4.** (a) Definition sketch for a stretch of coast characterized by a shoreline orientation  $\beta$  and affected by a wave propagating from  $\alpha$ ; (b) example of net littoral drift rose. The blue line denotes positive littoral drift, while the red line denotes negative littoral drift.

One of the major findings concerning the LDR concept [3] is that, in terms of littoral drift, the effects of a deep-water wave climate can be equated to a single equivalent wave component, with parameters  $H_{s0,eq}$ ,  $T_{p0,eq}$ , and  $\alpha_{0,eq}$ , i.e.,

$$Q(\beta) = \sum_{\alpha_{0i}=\beta-\frac{\pi}{2}}^{\alpha_{0i}=\beta+\frac{\pi}{2}} p_i \cdot \frac{K \cdot (H_{s0,i})^{2.4} \cdot (T_{p0,i})^{0.2} \cdot g^{0.6}}{16 \cdot (s-1) \cdot (1-n) \cdot \pi^{0.2} \cdot \gamma^{0.4} \cdot 2^{1.4}} \sin[2(\beta - \alpha_{0i})] \cong G_{eq} \cdot \sin[2(\beta - \alpha_{0,eq})], \quad (3)$$

where

$$G_{eq} = \frac{K \cdot (H_{s0,i})^{2.4} \cdot (T_{p0,i})^{0.2} \cdot g^{0.6}}{16 \cdot (s-1) \cdot (1-n) \cdot \pi^{0.2} \cdot \gamma^{0.4} \cdot 2^{1.4}}. \quad (4)$$

The equivalent wave direction  $\alpha_{0,eq}$  is easily detected from the LDR graph, as it corresponds to the null point, while wave height and period can be inferred from Equation (4) using (for example) common harmonic regression techniques, although a relationship between wave height and period needs to be established. Most notably, the equivalent direction parameter (equal to the LDR null point) is of significant importance in shoreline evolution forecast, as it is nothing but the dominant direction of wave climate that persistently affects and sculpts the shoreline over years. In practical coastal engineering, the total wave climate is in fact seldom reduced to the equivalent wave component in mid-long-term analysis of shoreline evolution, a procedure that has been widely applied in the literature, particularly in the field of static equilibrium crenulated bays [17].

Nevertheless, the main point of the present paper regards the fact that the “Total-LDR”, in most cases, is approximately equal to a single wave component coming from a constant direction (“Equivalent-LDR”). This feature can be discussed in terms of shore diffusivity.

According to [3,18,19], stable/unstable behavior of the coast can be interpreted via the shoreline “diffusion” equation. As stated by [20], the long-term shoreline evolution can be modeled by following a single contour line, with the main assumptions that the coast preserves an equilibrium profile, and that net cross-shore sediment movements are

negligible compared to gradients in alongshore sediment transport. With the conservation of mass and the chain rule, this yields the one-line contour equation (OLCE).

$$\frac{\partial y}{\partial t} = -\frac{1}{D_c + B} \frac{\partial Q}{\partial x} = -\frac{1}{D_c + B} \frac{\partial Q}{\partial \theta} \frac{\partial \theta}{\partial x'} \quad (5)$$

where  $y$  is the offshore direction,  $x$  is the shoreline position in the long-shore direction,  $D_c$  [21] is the closure depth,  $B$  is the average berm height, and  $\theta$  is the angle between the wave direction and the shoreline normal. Assuming that the shoreline has a mild curvature,

$$\frac{\partial \theta}{\partial x} = \frac{\partial^2 y}{\partial x^2}. \quad (6)$$

Combining with Equation (5), the shoreline diffusivity equation is obtained.

$$\frac{\partial y}{\partial t} = \pm \varepsilon(t) \frac{\partial^2 y}{\partial x^2}, \quad (7)$$

where  $\varepsilon(t)$  is the diffusivity coefficient, whose sign and magnitude are determined by the combination of the wave angle and shore characteristics. Specifically,  $\varepsilon(t)$  is a time-dependent coefficient, since the wave angle  $\theta(t)$  varies over time for a deep-water wave climate. Therefore, considering the common practice, within a mid-term shoreline analysis, of reducing the wave climate into the LDR equivalent wave component, only a constant time-averaged diffusivity,  $\hat{\varepsilon}$ , is accounted for, as all we do is mediate the diffusivity equation over time. Therefore, since both the first and the second terms of Equation (7) are time-dependent, it stands to reason to expand the  $\varepsilon(t)$  coefficient in a Taylor series.

$$\varepsilon(t) = \hat{\varepsilon} + \frac{\partial \varepsilon}{\partial t} dt + \dots \quad (8)$$

In light of this, if the wave sector is relatively small, it is possible to neglect the higher-order terms, and the shoreline diffusivity would consequently be constant over time. The latter consideration, in the context of the LDR concept, shows that the degree of approximation of the Total-LDR to a single wave component is nothing but the degree of approximation of the total shore diffusivity  $\varepsilon(t)$  to a constant one. In other words, the difference between Total- and Equivalent-LDR almost represents the difference  $\hat{\varepsilon} - \left[ \frac{\partial \varepsilon}{\partial t} dt + \dots \right]$ .

Accordingly, as long as the Total-LDR is approximately equal to the Equivalent-LDR (symmetrical lobes), a negligible effect of the time variation of wave climate on the diffusivity is observed. Obviously, this occurs when in narrower wave sectors, where the wave climate exhibits a single directional mode and a limited directional variance, as in many areas of the Tyrrhenian Sea (e.g., Figure 5).

Conversely, any deviation of the total LDR to the equivalent one (asymmetrical lobes) would denote an influence of the directional climate variability on the general diffusivity of the coast. This is exactly what happens for the Molise coast case study, as shown in the next section.

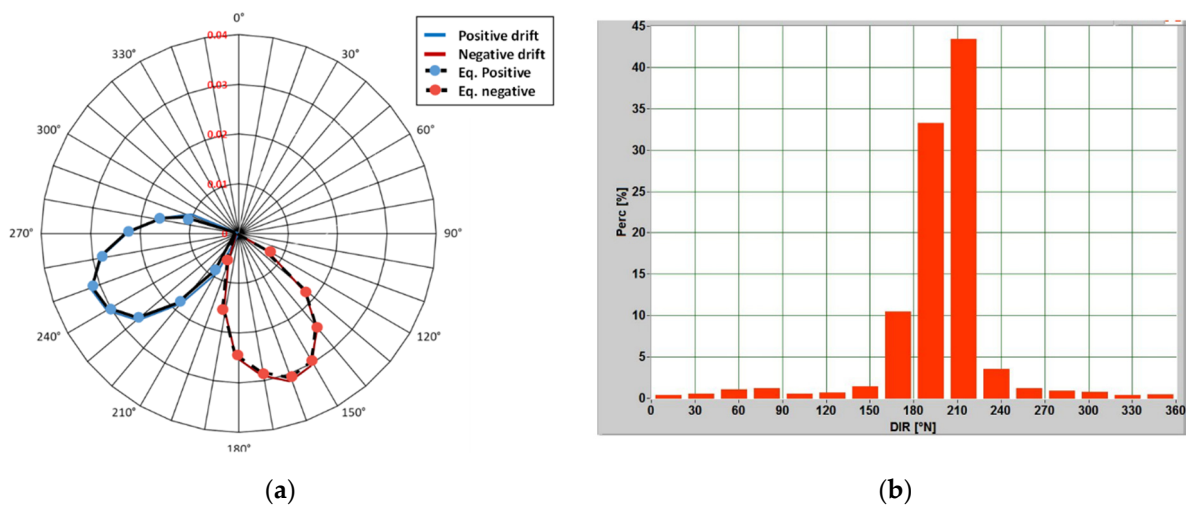


**Figure 5.** (a) Single-component approximation for Bagnoli Bay (Napoli); (b) histogram of wave directions.

### 3.2. Wave Climate and Littoral Drift Rose of Molise Coast

By applying Equation (2) to the deep-water Molise climate, inferred through the Ortona buoy, it was possible to reconstruct the LDR of Molise coast. Specifically, since the directional buoy located nearby the town of Ortona is nearly 56 km north from the mouth of Trigno river, homogeneous meteorological conditions affect both areas, thus leading to a reliable wave climate forecast. The main results of the wave climate analysis are summarized below.

#### 3.2.1. Molise Wave Climate

The Ortona buoy is located at a depth of approximately 70 m below the low-tide level, at a latitude of  $42^{\circ}24'54.0''$  N and a longitude of  $14^{\circ}30'20.99''$  E. Significant wave height,  $H_s$ , peak period,  $T_p$ , and azimuth of the mean wave direction,  $\alpha$ , were recorded in the period 1989–2012, at an average interval of 3 h. Wave heights and periods were adjusted to the sea offshore the Molise coast according to the relationships originally introduced by [22] in the frame of the JONSWAP project, while also assuming the same wind blowing at both locations [23].

Figure 6a shows the histogram of wave direction for angular sectors of  $22.5^{\circ}$  N, in which the offshore directed waves were removed for clarity. It can be seen that the wave climate is characterized by two well-defined modes: one is around  $350^{\circ}$  N, while the other is close to  $80^{\circ}$  N.

This behavior was observed to occur almost seasonally and monthly (Figure 6b,c), indicating an inherent bimodal climate that affects the Molise coast, where a frequent inversion of littoral transport direction can be expected. This second aspect is further supported by the graph shown in Figure 7, where a predominance of waves coming from  $340^{\circ}$  N is observed during warmer months, whereas waves originating from  $80^{\circ}$  N prevail during winter months.

From Figure 7, it can be seen that the waves in January and February, which may be included in the winter season, are dominant from  $350^{\circ}$  N. This anomaly in the winter dominant direction could be explained by the prevailing wave energy field and wind conditions. As reported by [10], although two modes ( $80^{\circ}$  N and  $350^{\circ}$  N) predominate within Molise climate, waves from ENE–E have a lower height; consequently, their wave energy is also lower. By contrast, higher energy values are found for a wave sector ranging between  $316^{\circ}$  N and  $45^{\circ}$  N. Since, in general, a greater amount of energy is associated with storm weather conditions (November–February), it is reasonable to expect the dominant direction to reverse and turn toward the greater energy.

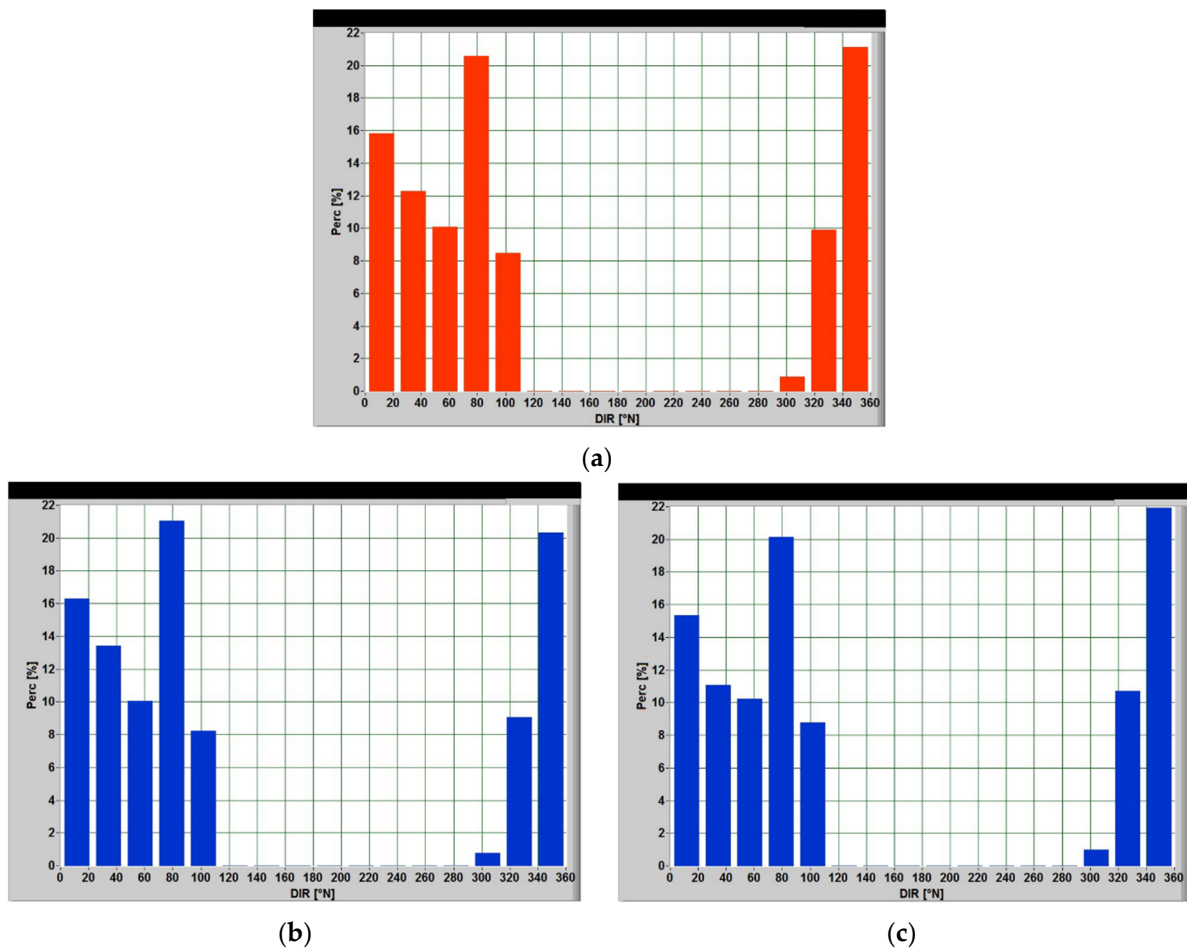


**Figure 6.** (a) Annual histogram of wave directions for angular sector of  $22.5^\circ$  for the Molise coast; (b) April to October histogram of wave directions for angular sector of  $22.5^\circ$  for the Molise coast; (c) October to April histogram of wave directions for angular sector of  $22.5^\circ$  for the Molise coast. Onshore directed angles were removed.

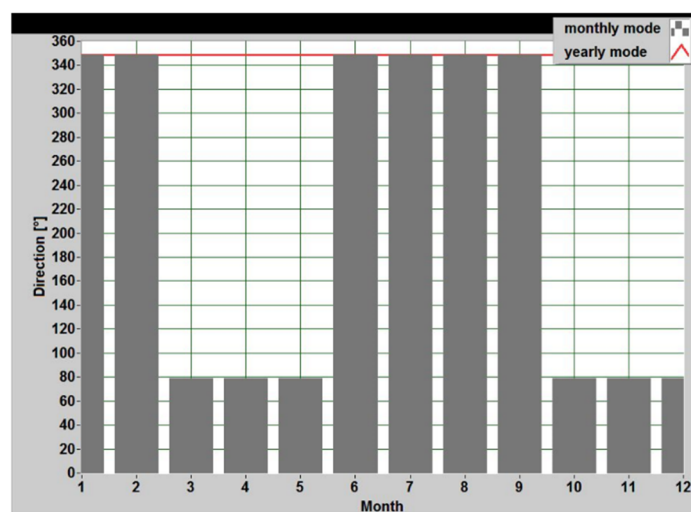


**Figure 7.** Monthly variation of the Molise wave climate directional mode.

### 3.2.2. Molise LDR

The LDR for the Molise climate is shown in Figure 8a. It can be seen that the “positive lobe” (littoral drift rightward) is located right of the negative one (littoral drift leftward). Moreover, the equivalent wave parameters were estimated from the Molise LDR graph;

the equivalent wave direction was equal to  $9^\circ$  N, corresponding to the null point of the real LDR, while the equivalent wave height and period were fitted to have the same littoral transport magnitude, yielding  $H_{s0,eq} = 0.83$  m and  $T_{p0,eq} = 5.08$  s. It is surprising to observe how the equivalent wave direction of  $9^\circ$  N corresponds to that of  $10^\circ$  N empirically detected by [10] simply observing the shoreline trend of the undefended stretch of coast near the Saccione stream mouth.

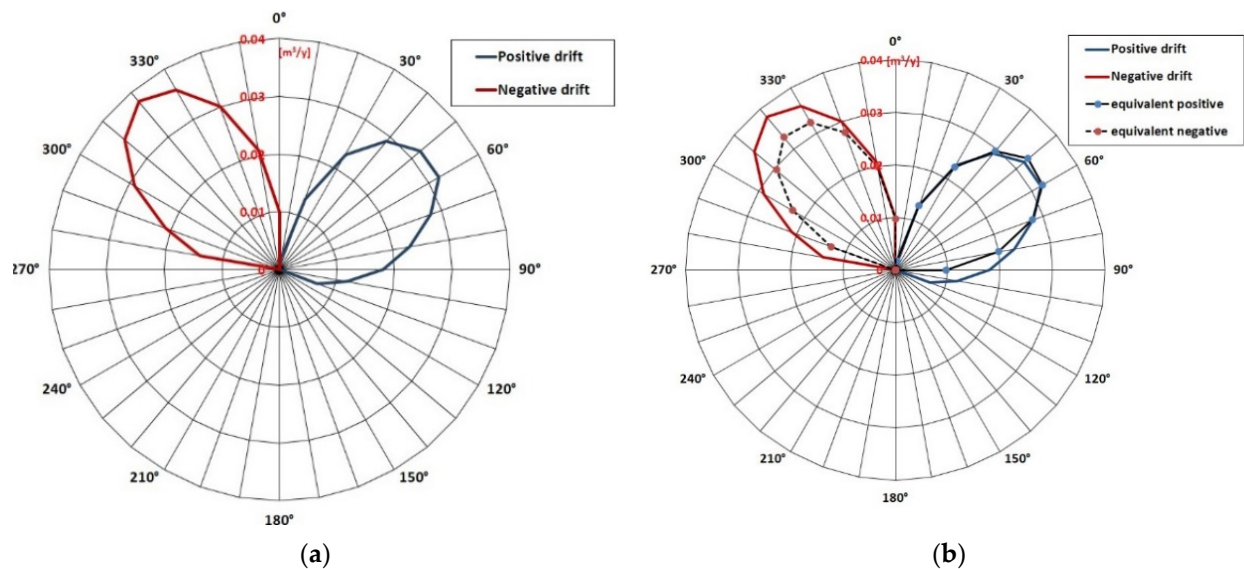


**Figure 8.** (a) Net littoral drift rose of Molise coast; the blue line represents drift to right when looking offshore, while the red line represents drift to left when looking offshore; (b) comparison between Total- and Equivalent-LDRs of Molise coast. Littoral drift in cubic meters per year.

In Figure 8b, the Total-LDR and Equivalent-LDR are compared. It can be seen that, due to the inherent bimodality of the local wave climate, the Total-LDR of Molise coast showed asymmetrical lobes, with the negative lobe being greater than the positive one. For a wave climate to be satisfactorily approximated by a single wave component, it is necessary for the Total-LDR to have nearly symmetrical lobes. This normally occurs in monomodal climates with a limited directional variance. Conversely, with widely varying wave directions, as in the case of the Adriatic Sea here presented, a weak fit is achieved. As a matter of fact, the Molise “equivalent wave” is not able to wholly approximate the littoral rose, and it properly fits only the part of the rose included between  $340$  and  $70^\circ$  N.

In summary, on the one hand, a proper fit of the Total-LDR by a single component indicates a constant shore diffusivity in the mid-term. This is obvious whenever the wave climate is coming from a restricted angle. For the case study here presented, the observed poor approximation of the Total-LDR to the equivalent one would indicate that the Molise coast diffusivity is not constant over time, thus denoting that the higher-order terms of Equation (8) are not negligible, since the directional variability of wave climate is significantly large. This aspect could represent a limitation within a mid-term analysis of coastal evolution based on the equivalent wave concept. The latter could result not significant in forecasting shoreline evolution due to its inability to account for the time-varying diffusivity extra effect.

Therefore, in the present paper, we firstly tried to quantify the explanatory power of the LDR equivalent wave and its significance within a bimodal climate; secondly, we tried to assess the effect of an inconstant diffusivity on the shoreline response. Specifically, the second feature was achieved by considering the  $\frac{\partial \xi}{\partial t}$  terms of Equation (8) on the basis of two different time-resolved equivalent climates, namely, an equivalent climate with a monthly time scan and an equivalent frequency-based climate with a 6 h time scan.

### 3.2.3. Monthly LDR-Equivalent Wave Climate

Where a strong directional variability is observed, there might be the chance of a monthly (or seasonal) inversion of the equivalent direction of waves.

As discussed in [2], in fact, the LDR null point can change its position over the year. In such situations the annual equivalent wave representation could be “split” into monthly varying LDRs, thereby obtaining monthly equivalent wave parameters (wave height, wave period, and wave direction). To this aim, monthly LDRs were reconstructed from Molise wave climate, and, from them, equivalent wave components were obtained.

A wave time series can be built using monthly varying equivalent sea state parameters, which repeat themselves year per year. For the Molise climate, the equivalent direction is reversed every month, as depicted in Figure 9; therefore, the time-varying diffusivity effect changes over time with a resolution of 1 month.

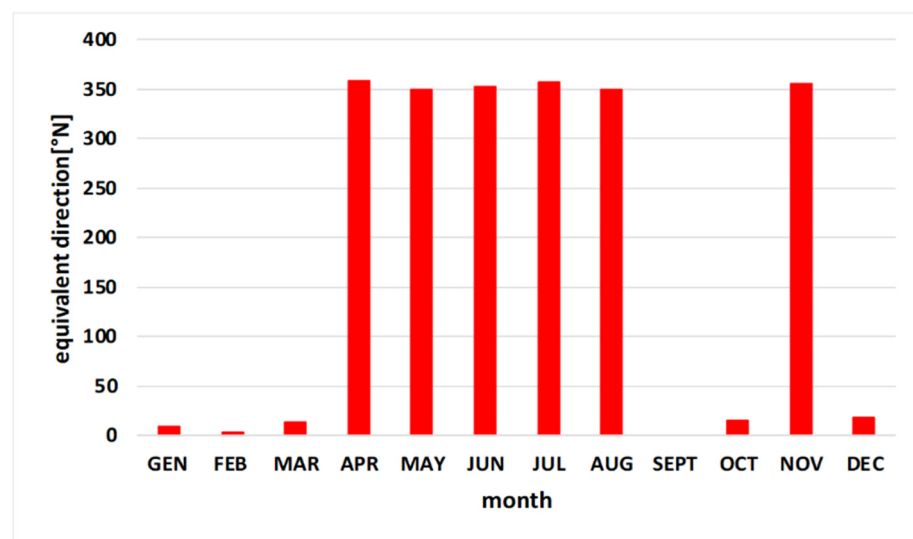


Figure 9. Monthly variation of the LDR equivalent direction of Molise climate.

### 3.2.4. Frequency-Equivalent Wave Climate

According to the initial distribution approach [24], wave information was firstly used to build up a sea–climate matrix. Wave data were grouped into angular sectors  $10^\circ$  N wide (0 to  $350^\circ$ ) and, for each sector, 20 wave height classes were considered, between 0 and 10 m; each wave height class was provided with its frequency of occurrence and the corresponding average of peak periods,  $\bar{T}_p$ .

A statistically equivalent series of wave attacks was then achieved from the sea–climate matrix, assuming wave directions to be random variables uniformly distributed between  $0^\circ$  N and  $350^\circ$  N. For each wave direction, 20 wave attacks were used, with significant wave height corresponding to the center of the wave height classes and peak period equal to  $\bar{T}_p$ . Each event was supposed to have a yearly duration equal to the frequency of occurrence of the corresponding wave class. Notably, the procedure was repeated year by year, implying that the sequence of wave directions changes from 1 year to another.

In the application discussed below, durations less than 6 h were discarded since their effect on the mid-term shoreline evolution was assumed negligible.

## 3.3. Numerical Study

### Software, Boundary Conditions and Model Parameters

The numerical analysis carried out herein employed the popular software GENESIS (Generalized Model for Simulating Shoreline Changes), the properties of which have been well discussed in several studies. GENESIS integrates the OLCE, Equation (2), and allows accounting for the presence of coastal structures, which may transmit waves in the sheltered area by either wave breaking [25] or overtopping (among others [26–28]).

In GENESIS, the littoral drift is computed empirically, as a function of the breaking wave parameters (height, period, and angle) and two transport coefficients,  $K_1$  and  $K_2$ . The former account for sand transport caused by obliquely incident waves [16] and correspond to the  $K$  empirical parameter of the CERC formula (Equation (2)), while the latter are related to an additional phenomenon causing long-shore transport: the effect of alongshore wave gradients associated with the presence of diffractive structures. It is important to point out that, despite the empirical genesis of  $K_1$  and  $K_2$ , they are treated as calibration parameters of the numerical model, in order to overcome the many assumptions of the model and to account for the actual littoral transport.

As such, the solution of Equation (2) is determined according to the knowledge of the following quantities:

1. Initial shoreline,  $y_0(x)$ ;
2. Lateral boundary conditions;
3. Structure characteristics;
4. Transport coefficients;
5. Values of  $D_c$  and  $D_B$ ;
6. Wave climate.

The shoreline position at 2004 was used as the initial condition; original data were passed through a Godin filter with a 1000 m window width, to smooth out any abrupt changes in the shore orientation (Figure 10). The Godin filter was selected as it is rather steep and induces no oscillations at the reach bounds [29].

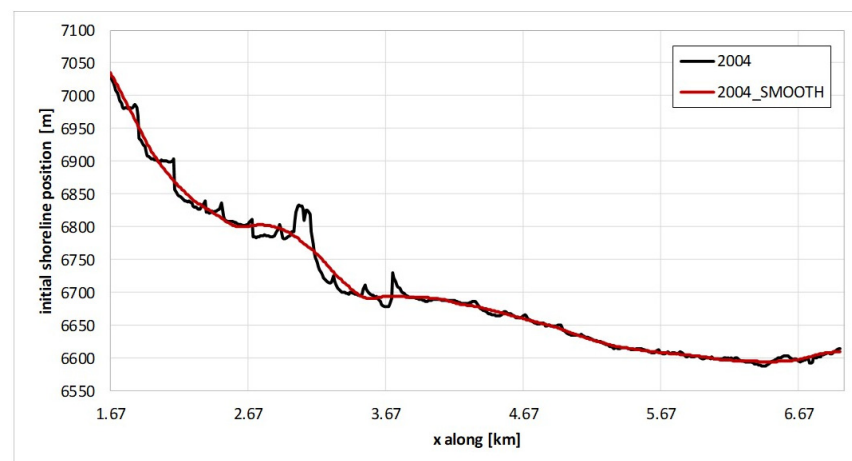


**Figure 10.** Shoreline position in 2004; the black line represents the unsmoothed coastline position, and the red line represents the smoothed coastline position.

Lateral boundary conditions were assigned by tentatively assuming that the “zero *LRR* sections” bounding the study area (Figure 3) were “pinned”, i.e., underwent no variations in the shoreline position at any instant in time. Both the jetty, which armors the Trigno estuary, and the groins located southward (Figure 11) were reproduced in GENESIS with the same length and mutual distance as in real life. To reduce the degrees of freedom in the numerical simulations, all structures were assumed nondiffractive ( $K_2 = 0$ ), such that the solution of OLCE depended upon the transport coefficient  $K_1$  (referred to hereafter as  $K$ ) and the permeability of structures  $P$ .

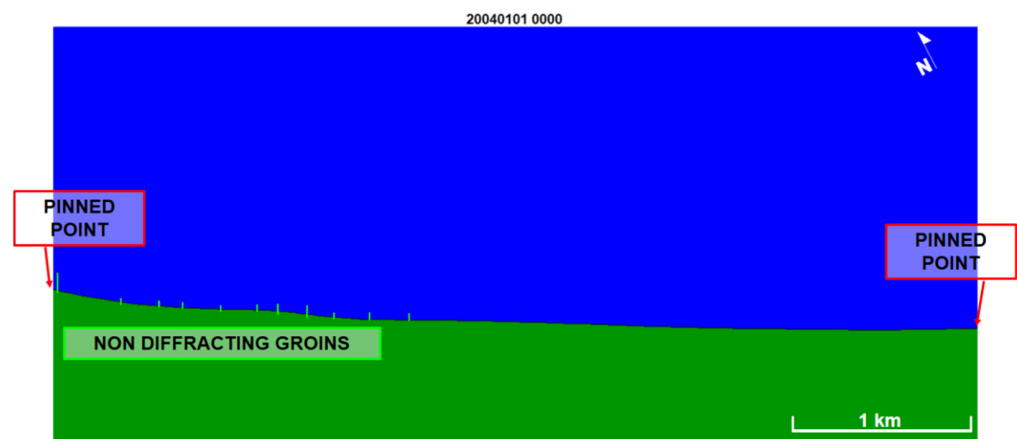


**Figure 11.** GENESIS configuration of the modeled area. All structures defending the area since 2004 were reproduced with the same length and mutual distance.

Both the above quantities were treated as calibration parameters, under the only constraint that their value was physically consistent. As per  $K$ , a previous application of OLCE to the Molise coast suggested an order of magnitude value of 0.1; hence, the range 0.04–0.3 was (somewhat subjectively) chosen. Otherwise,  $P$  was varied in the reasonable interval 0–0.3 and was supposed to attain the same value for all structures. According to the early literature [6,10], the depth of closure was equated to 9.4 m, while the active berm height was set at 1.5 m.

The dependence of the shoreline response on wave climate (particularly wave direction) was the core of this article, and the results are broadly discussed in Section 4.

## 4. Results

### 4.1. Annual LDR-Equivalent Wave Climate

First of all, in order to test the degree of correlation of the dominant wave attack for littoral transport with the coastline evolution, the LDR-equivalent wave was inputted into the model GENESIS in the form of a 12 year (2004–2016) time series. Different model scenarios were created by varying the transport coefficient  $K$  and the groin permeability  $P$ . The shorelines outputted from the GENESIS model were used to calculate the “LRR predicted function”, which was then compared with the “LRR measured function” (Figure 4) of the Trigno mouth area.

To measure the model performance, two prediction indices were used:

- the  $R^2$  statistics, indicating the correlation between measured and predicted LRR;
- the relative mean square error (RMSE), given by

$$RMSE = \sqrt{\frac{\sum_{i=1}^N (LRR_{meas_i} - LRR_{pred_i})^2}{N}}, \quad (9)$$

where  $N$  is the total number of the shoreline position, while  $LRR_{meas}$  and  $LRR_{pred}$  are the accretion/erosion indices measured and predicted, respectively.

Figure 12 shows the superimposition of the RMSE surface and the  $R^2$  contour lines obtained by the comparison between the measured and predicted LRR functions of each model scenario. The best performance (maximum  $R^2$  and minimum RMSE) was found at a groin permeability  $P$  of 0.2 and a  $K$  value of 0.2. The graph showed a good prediction power of the equivalent wave, as it was able to account for about 90% of the total Trigno LRR variance.

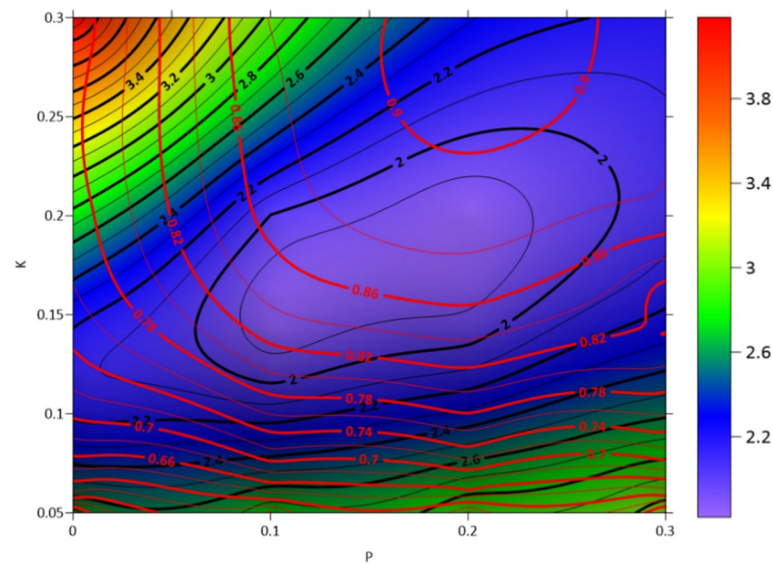


**Figure 12.** Superimposition of the  $RMSE$  surface (black contour lines) and the  $R^2$  surface (red contour lines) for the annual LDR-equivalent climate ( $9^\circ$  N). The  $x$ -axis is the groin permeability  $P$ , while the  $y$ -axis is the GENESIS transport coefficient  $K$ . Surfaces were obtained by comparing the “measured” and “predicted”  $LRR$  functions of each  $K$ – $P$  scenario.

Nevertheless, the  $RMSE$  and the  $R^2$  surfaces were not “in phase”; in fact, contours had an initial subparallel pattern, but with the  $RMSE$  decreasing faster than the  $R^2$  increasing with the  $K$  parameter. Therefore, the surfaces attained the absolute maximum of  $R^2$  and the absolute minimum of  $RMSE$  in separate areas of the  $K$ – $P$  space.

Moreover, it should be noted that, in the best scenario, the  $RMSE$  value was relatively large; however, the absolute minimum ranged between 1.5 and 2 months/year, which was considerably higher than the expected error given by the shoreline surveys (Table 1). Therefore, in order to test if the equivalent wave parameters returned the best prediction of the Trigno shoreline evolution, we first carried out a significance analysis of the equivalent direction by varying the angle  $\pm 30^\circ$  with respect to  $9^\circ$  N.

The best performances for the seven equivalent directions analyzed are summarized in Figure 13, highlighting that the maximum  $R^2$  and minimum  $RMSE$  lay between  $\pm 10^\circ$  around the equivalent LDR direction of  $9^\circ$  N. Specifically, it can be noted that, for the three best equivalent directions of  $0^\circ$  N,  $9^\circ$  N, and  $20^\circ$  N, the values attained by the performance indices were very close to each other. The observed invariance confirmed that the LDR-equivalent direction of  $9^\circ$  N was well correlated with the real shoreline trend, and it can be trustily used in medium–long-term shoreline analysis.

Nevertheless, the numerical model systematically overestimated the real average trend of the coast. Figure 14 (panel (a)  $0^\circ$  N; panel (b)  $9^\circ$  N; panel (c)  $20^\circ$  N) shows the surface representing the difference between the arithmetic mean of measured and calculated  $LRR$ ; the null values of this difference were not found for the best  $K$ – $P$  scenarios (as expected); rather, there was an average systematic overestimation of around 1–1.5 m.

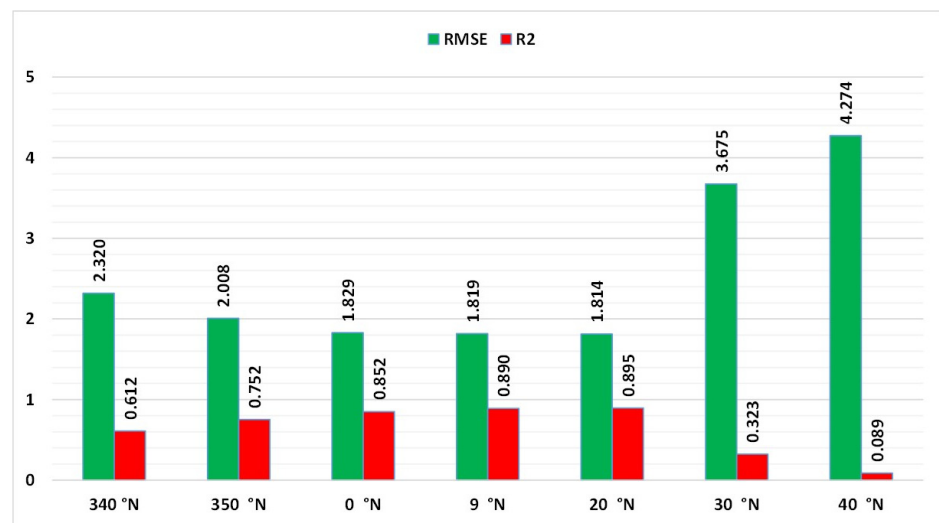


**Figure 13.** Best performance indices ( $R^2$  and  $RMSE$ ) for the seven equivalent directions analyzed within the LDR-equivalent direction significance study. Values were obtained by comparing the “measured” and “predicted”  $LRR$  functions.

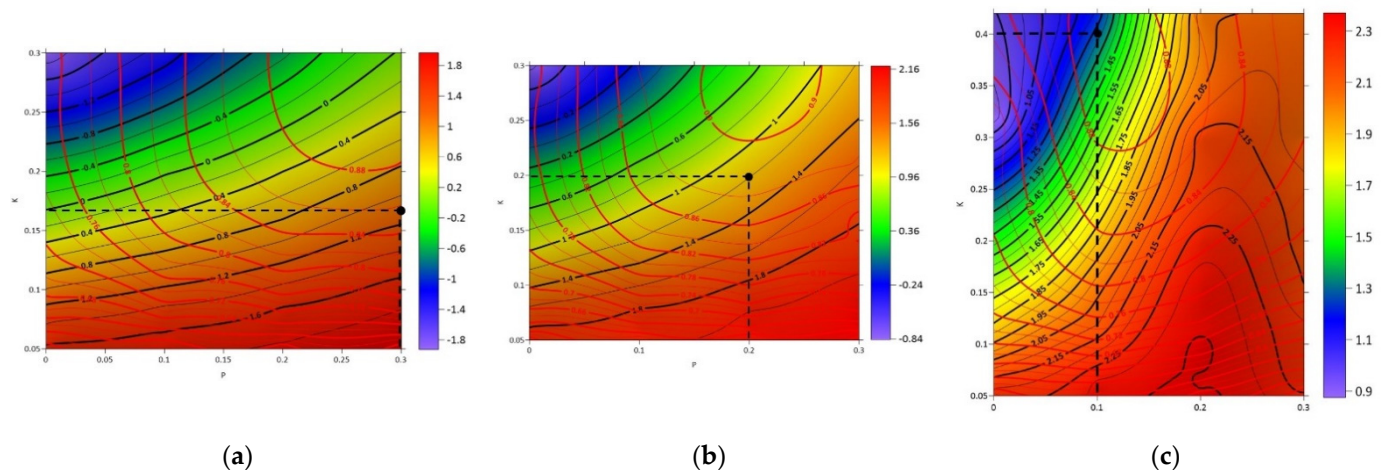


**Figure 14.** Comparison of difference between the arithmetic mean of measured and calculated  $LRR$  surface (black contour lines) and  $R^2$  surface (red contour lines): (a)  $0^\circ$  N; (b)  $9^\circ$  N; (c)  $20^\circ$  N. The  $x$ -axis is the groin permeability  $P$ , while the  $y$ -axis is the GENESIS transport coefficient  $K$ . Black dashed lines indicate the  $K$ - $P$  scenarios with the best performance (minimum  $R^2$ , maximum  $RMSE$ ).

The reasons for this underlying bias produced by the annual equivalent wave component can likely be found, at first glance, in the influence of the more angled climate components. This can be outlined by separately observing the area covered by groins (first 2 km) and the remaining unprotected 3 km reach of coast. Figure 15 shows the  $LRR$  functions for the three best equivalent directions ( $0^\circ$  N,  $9^\circ$  N, and  $20^\circ$  N). In the protected area, the overestimation was reduced moving toward  $0^\circ$  N; on the contrary, in the unprotected area, it was reduced moving toward  $20^\circ$  N. This seems to confirm that the equivalent direction varied and was reversed over time, a predictable behavior when in bimodal wave climate conditions.

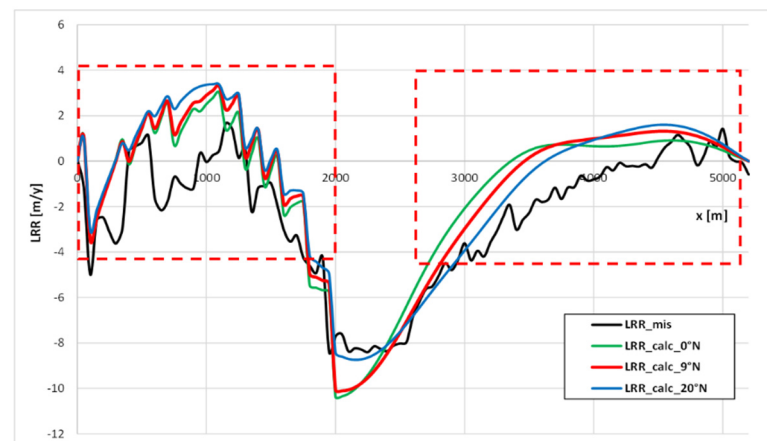


**Figure 15.** *LRR* functions for the three best equivalent directions ( $0^\circ$  N,  $9^\circ$  N, and  $20^\circ$  N) compared with the *LRR* measured function of the Trigno area. Red dashed boxes indicate the two subareas where an overestimation was observed: the left one (first 2 km) was located within the groin area, while the second one was located within the unprotected zone (last 3 km).

By strictly focusing on the groins area (Table 2), it can be noted that the more angled directions produced a bias reduction; in fact, the *RMSE* and the mean were the lowest, confirming that the reversal of the equivalent direction would influence the predicted shoreline trend. However, the correlation index remained relatively low for  $340^\circ$  N and  $350^\circ$  N, and it tended to increase moving toward the LDR-equivalent direction, attaining 70% of the explained variance.

**Table 2.** Groin area performance indices (*RMSE*,  $R^2$ , and mean  $\mu$ ) for the best scenario for the shifted direction.

DD ( $^\circ$ N)	<i>P</i>	<i>K</i>	<i>RMSE</i> (Months/Year)	$R^2$	$\mu$ (Months/Year)
340	0.3	0.1	2.091	0.503	1.122
350	0.3	0.12	2.034	0.601	1.169
0	0.3	0.16	2.138	0.689	1.418
9	0.2	0.2	2.301	0.709	1.699
20	0.1	0.4	2.546	0.714	1.528
30	0	0.16	2.839	0.114	1.772
40	0.3	0.05	3.900	0.302	1.062

To sum up, the significance analysis of the equivalent direction confirmed that, by reducing the total wave climate to a single equivalent wave component, consequently accounting for a constant value of the shore diffusivity, the LDR-equivalent wave was significantly better correlated to the real shoreline trend, although a biased result was produced. However, the fact that the more angled components were found to act on the bias, as shown in Table 2, suggests that it is not possible to neglect the directional variability of wave climate. Therefore, in order to evaluate climate reversal, a time-varying diffusivity extra effect on shoreline response was considered within the analysis. Two different wave climate resolutions were inputted into the GENESIS model: the monthly LDR-equivalent climate and the frequency-equivalent time series.

#### 4.2. Monthly LDR-Equivalent Wave Climate

The role of the monthly representation of LDR was analyzed mainly because of the likely annual inversion of the equivalent direction in a bimodal wave climate (Figure 9). In this case, GENESIS scenarios were set by inputting a 12 year wave time series with a monthly variation of the equivalent parameters: direction, wave height, and wave period.

Figure 16 shows the superimposition of the  $RMSE$  surface and the  $R^2$  contour lines obtained by the comparison between the measured and predicted  $LRR$  functions for each model scenario. With respect to the results obtained with the annual equivalent component (Figure 12), the monthly scan of wave climate also showed a good prediction power, and the best performance (maximum  $R^2$  and minimum  $RMSE$ ) was found at a groin permeability  $P$  of 0.2 and a  $K$  value of 0.2 (Table 3).

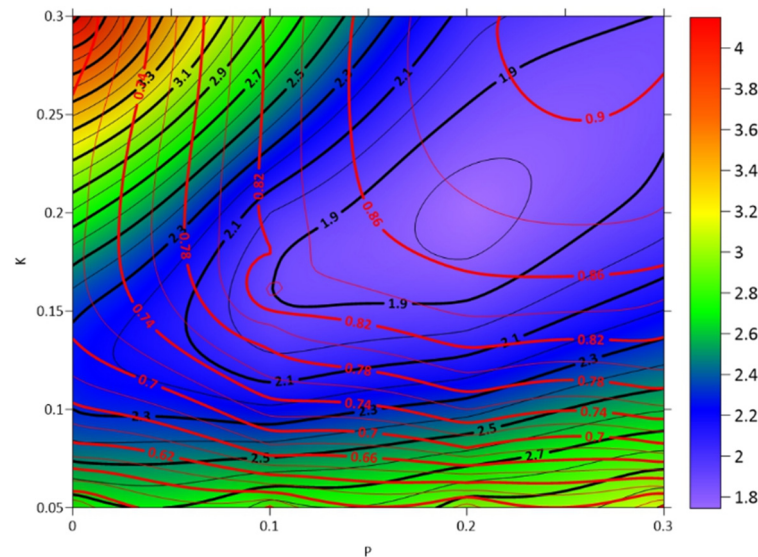


**Figure 16.** Superimposition of the  $RMSE$  surface (black contour lines) and the  $R^2$  surface (red contour lines) for the monthly LDR-equivalent climate. The  $x$ -axis is the groin permeability  $P$ , while the  $y$ -axis is the GENESIS transport coefficient  $K$ . Surfaces were obtained by comparing the “measured” and “predicted”  $LRR$  functions of each  $K$ – $P$  scenario.

**Table 3.** Performance indices ( $RMSE$ ,  $R^2$ , and mean  $\mu$ ) for the monthly LDR-equivalent climate.

$P$	$K$	$R^2$	$RMSE$ (Months/Year)	$\mu$ (Months/Year)
0	0.12	0.6841	2.248	1.23
0.1	0.16	0.8449	1.902	1.13
0.2	0.2	0.8766	1.743	1.20
0.3	0.2	0.9041	1.896	1.17

As noted, by comparing the performance indices, the monthly equivalent climate produced a slight reduction in the  $RMSE$  (from 1.819 to 1.743 months/year), while the  $R^2$  was still high but slightly lower (from 0.89 to 0.876). In a nutshell, there was no appreciable improvement in the predicted shoreline trend. Furthermore, an overestimation was still found in the initial and final parts of the study area, and the arithmetic residual mean was still 1.20 months/year.

In addition, focusing on the groin area for the best monthly scenario ( $P = 0.2$  and  $K = 0.2$ ), the prediction remained quite the same, with no tangible improvement; specifically, the correlation was the same, while a little bias reduction of 0.2 m/year was detected.

#### 4.3. Frequency-Equivalent Time Series

A 12 year frequency-equivalent time series was inputted in the GENESIS model, where the wave height, wave period, and wave direction variation were forecasted according to the frequency of appearance of the real Molise wave climate, thus obtaining a more accurate climate representation able to account for both climate reversal and, to some extent, extreme events produced by storms.

The results are shown in Figure 17 and Table 4. The best prediction was obtained with a groin permeability of 0.2 and a transport coefficient of 0.46. It can be noted that, similarly to the monthly climate, an increased scan of wave climate produced a bias reduction and, at the same time, a slight reduction in the degree of correlation, which was still really high ( $R^2 = 0.835$ ). By comparing these results to the other two climate resolutions (annual and monthly equivalent climates), the frequency-equivalent time series was seemingly the best prediction model, due, in particular, to the greatest bias reduction ( $RMSE = 1.5$  months/year and  $\mu = 0.7$  months/year).

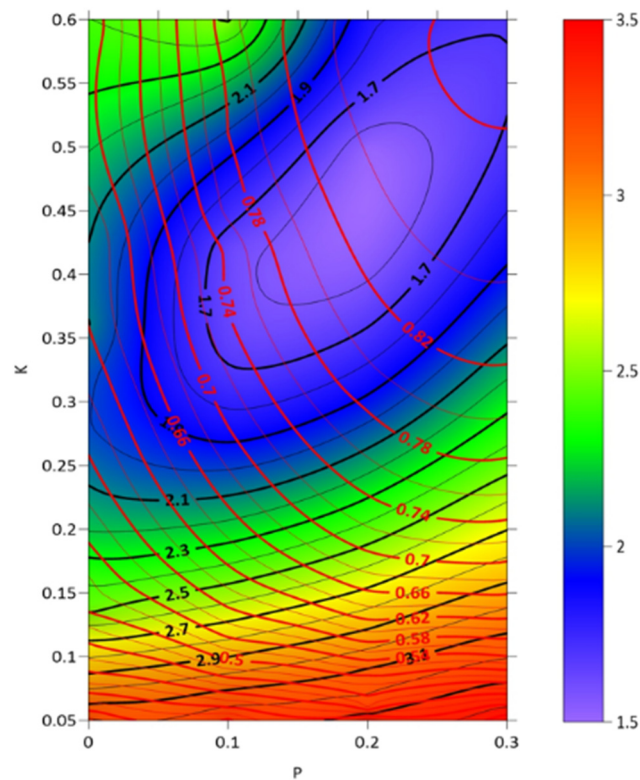


**Figure 17.** Superimposition of the  $RMSE$  surface (black contour lines) and the  $R^2$  surface (red contour lines) for the frequency- equivalent climate. The  $x$ -axis is the groin permeability  $P$ , while the  $y$ -axis is the GENESIS transport coefficient  $K$ . Surfaces were obtained by comparing the “measured” and “predicted”  $LRR$  functions of each  $K$ - $P$  scenario.

**Table 4.** Performance indices ( $RMSE$ ,  $R^2$ , and mean) for the frequency-equivalent climate.

$P$	$K$	$RMSE$ (Months/Year)	$R^2$	$\mu$ (Months/Year)
0	0.36	2.105	0.620	0.081
0.1	0.38	1.643	0.744	0.519
0.2	0.46	1.519	0.835	0.721
0.3	0.55	1.693	0.864	1.054

Nevertheless, a more accurate analysis shows that the effect of the equivalent time series on the model was a simple translation of the calculated trend toward the measured value, likely determined by the effect of the extreme waves, which produced, by contrast, a reduction in the correlation. The paradigmatic example can be shown by restricting the attention to the area defended by groins. As shown in Figure 18 and in Table 5, a narrower climate resolution led to a more unbiased numerical model, but a lower correlation ( $R^2$ ). In fact, although LDR results appeared very biased, a correlation of around 70% was observed; by contrast, the very opposite occurred for the frequency-equivalent climate. In this case,

the bias was reduced but the correlation coefficient dramatically decreased by 20 points (Table 5).

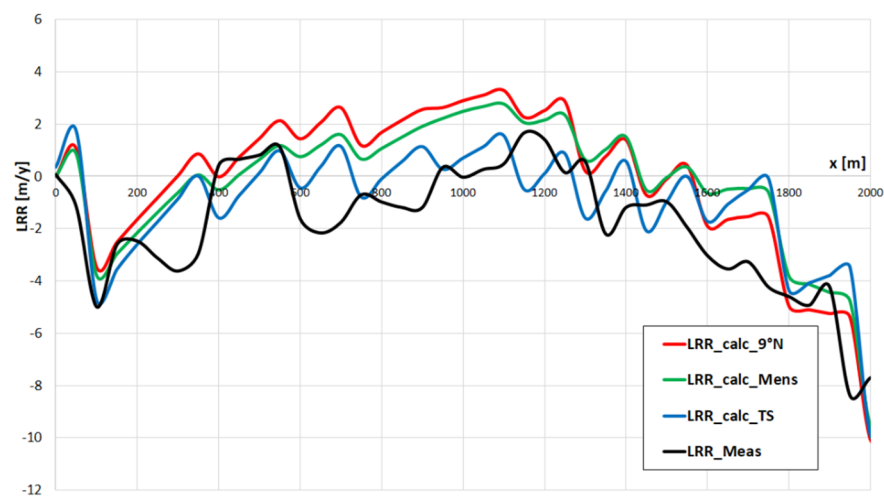


**Figure 18.** Focus of the *LRR* functions within the groin area (2 km) for the three different climate time resolutions analyzed.

**Table 5.** Comparison of annual LDR-equivalent climate, monthly LDR-equivalent climate, and frequency-equivalent climate.

Climate	<i>P</i>	<i>K</i>	<i>RMSE</i> (Months/Year)	<i>R</i> <sup>2</sup>	$\mu$ (Months/Year)
Annual LDR (9° N)	0.2	0.2	2.301	0.709	1.699
Monthly LDR	0.2	0.2	2.112	0.688	1.574
Frequency EQ	0.2	0.46	1.897	0.505	0.830

## 5. Discussion and Conclusions

A medium-term shoreline change study of the Trigno river mouth area (Molise region, Adriatic Sea) was presented, with the purpose of quantitatively testing the degree of correlation between the wave climate and shoreline response. This study was based on the assumption that a dominant wave attack for littoral transport exists, and that its parameters, wave height, wave period, and wave direction can be estimated through the littoral drift rose. Starting from the Molise wave climate, the LDR graph of Molise coast was assessed, and the equivalent wave parameters were estimated. Specifically, the Molise LDR exhibits an asymmetrical configuration due to the strong bimodality of the climate. It may be assumed that a better fit of the equivalent wave to the Total-LDR reflects greater equivalence of the total diffusion of the shoreline to a constant one. Any deviation between the Total-LDR and Equivalent-LDR may suggest that the directional variance influences the shoreline diffusion, which results in a time-varying diffusion extra effect. This situation corresponds to the Molise coast case of study.

Therefore, a numerical study was carried out using the one-contour line model GENESIS in order to (1) assess the explanatory power of the LDR equivalent wave and its significance within a bimodal climate, and (2) check the effect of a time-varying diffusivity on the shoreline response. In this regard, the reliability of the equivalent wave in forecasting a shoreline response in a bimodal climate has never been investigated in the literature, and, in addition, the effect of an expected time-varying diffusion has never been considered.

The first aim was examined by inputting within the GENESIS model an “annual scanned” 12 year time series built from the equivalent wave of Molise coast. The analysis was conducted by comparing the “LRR predicted function” with the “LRR measured function” of the Trigno mouth area, using  $R^2$  and  $RMSE$  as model performance indicators. Results showed that the LDR-equivalent direction of  $9^\circ$  N was strongly correlated to the real shoreline trend, as it was able to account for about 90% of the total Trigno LRR variance, even if the  $RMSE$  index was relatively large (about 1.8 months/year).

Additionally, a significance analysis of the equivalent direction was carried out by shifting the annual direction by  $\pm 30^\circ$ . It was proven that the best prediction power was included within  $\pm 10^\circ$  with respect to  $9^\circ$  N, thus confirming that the LDR null point is a good estimator of the shoreline trend, which can be trustily used in medium–long-term coastal analysis. Nevertheless, a systematic overestimation of the real shoreline trend was detected; the “annual climate” produced a bias of about 1–1.5 months/year, mainly concentrated in the initial (groin area) and final parts (unprotected area) of the Trigno stretch of coast. As far as the groin area is concerned, the more angled components ( $340^\circ$  N and  $350^\circ$  N) were found to act on the bias, suggesting that it is not possible to neglect the directional variability of wave climate, resulting in a time-varying diffusivity extra effect on shoreline response.

To this second aim, two different wave climate resolutions were inputted in the GENESIS model, the “monthly LDR-equivalent climate” and the “frequency-equivalent time series”. It is important to highlight that, while a monthly scan only represents the seasonal inversion of dominant direction, the frequency-equivalent time series is able to consider, to some extent, the effects of storms waves on the coastal evolution.

In summary, the explanatory power of the reduced climate scans, which accounted for the time-varying shore diffusivity  $\frac{\partial \xi}{\partial t}$ , was surprisingly lower than the LDR component one. It was noted that the time-varying shore diffusivity did not affect the shoreline trend; in fact, the correlation was drastically lower within the groin area, but it was able to have an influence on the bias. Such results indicate a doubtful role of the time-varying diffusivity. Nevertheless, since the frequency-equivalent climate, to some extent, accounts for extreme waves, it is clear that the effect was a local translation of the coastline, which tended to deviate from the long-term trend. It is worth highlighting that the bias could be related to physics phenomena (storms events) or due to different factors, such as the boundary conditions of the GENESIS model or the nonuniform shoreline trend over years [10]. However, these aspects deserve more research and will be investigated in future studies.

In conclusion, the results confirmed the reliability of the equivalent wave approach, even within a bimodal climate. Moreover, the possible effect of a time-varying diffusion, which is expected with a large directional variability, produced insignificant results with respect to the equivalent wave concept. Nevertheless, the possible effect of diffusion should be accurately modeled and investigated in future research works.

**Author Contributions:** M.C.C., writing, numerical simulations, data processing, and data analysis; M.B., writing, numerical simulations, data processing, and data analysis; G.D.P., data collection, writing, and data analysis; S.T., data analysis and writing; M.C., data collection, data analysis, and writing. All authors read and agreed to the published version of the manuscript.

**Funding:** This research received no external funding.

**Conflicts of Interest:** The authors declare no conflict of interest.

## References

1. Hanson, H.; Kraus, N.C. GENESIS: A Generalized Shoreline Change Numerical Model for Engineering Use. Ph.D. Thesis, University of Lund, Lund, Sweden, 1989.
2. Walton, T.L.; Dean, R.J. Application of Littoral Drift Roses to Coastal Engineering Problems. In Proceedings of the Conference on Engineering Dynamics in the Surf Zone, Institution of Engineers, Sydney, Australia, 14–17 May 1973; pp. 221–227.
3. Walton, T.L.; Dean, R.J. Longshore Sediment Transport Via Littoral Drift Rose. *Ocean. Eng.* **2010**, *37*, 228–235. [[CrossRef](#)]

4. Roszkopf, C.M.; Di Paola, G.; Atkinson, D.E.; Rodriguez, G.; Walker, I.J. Recent shoreline evolution and beach erosion along the central Adriatic coast of Italy: The case of Molise region. *J. Coast. Conserv.* **2018**, *22*, 879–895. [[CrossRef](#)]
5. Aucelli, P.P.C.; Di Paola, G.; Rizzo, A.; Roszkopf, C.M. Present day and future scenarios of coastal erosion and flooding processes along the Italian Adriatic coast: The case of Molise region. *Environ. Earth Sci.* **2018**, *77*, 371. [[CrossRef](#)]
6. De Vincenzo, A.; Covelli, C.; Molino, A.J.; Pannone, M.; Ciccaglione, M.C.; Molino, B. Long-term Management Policies of Reservoirs: Possible Re-use of Dredged Sediments for Coastal Nourishment. *Water* **2019**, *11*, 15. [[CrossRef](#)]
7. Molino, B.; Bufalo, G.; De Vincenzo, A.; Ambrosone, L. Semiempirical Model for Assessing Dewatering Process by Flocculation of Dredged Sludge in an Artificial Reservoir. *Appl. Sci.* **2020**, *10*, 3051. [[CrossRef](#)]
8. Covelli, C.; Luigi, C.; Pagliuca, D.N.; Molino, B.; Pianese, D. Assessment of Erosion in River Basins: A Distributed Model to Estimate the Sediment Production over Watersheds by a 3-Dimensional LS Factor in RUSLE Model. *Hydrology* **2020**, *7*, 13. [[CrossRef](#)]
9. Di Paola, G.; Ciccaglione, M.C.; Buccino, M.; Roszkopf, C.M. Influence of Hard Defence Structures on Shoreline Erosion Along Molise Coast (Southern Italy): A Preliminary Investigation. *Rend. Online Ital. (ROL)* **2020**, *52*, 2–11. [[CrossRef](#)]
10. Buccino, M.; Di Paola, G.; Ciccaglione, M.C.; Roszkopf, C.M. A Medium-Term Study of Molise Coast Evolution Based on the One-Line Equation and “Equivalent Wave” Concept. *Water* **2020**, *12*, 2831. [[CrossRef](#)]
11. Draper, N.R.; Smith, H. *Applied Regression Analysis*; John Wiley and Sons: Hoboken, NJ, USA, 1985.
12. Aucelli, P.P.C.; Izzo, M.; Mazzarella, A.; Roszkopf, C.M.; Russo, M. L’evento meteorico estremo di gennaio 2003 sul Molise. *Quad. Geol. Appl.* **2004**, *11*, 101–119.
13. Scorpio, V.; Aucelli, P.P.C.; Giano, S.I.; Pisano, L.; Robustelli, G.; Roszkopf, C.M.; Schiattarella, M. River channel adjustments in Southern Italy over the past 150 years and implications for channel recovery. *Geomorphology* **2015**, *251*, 77–90. [[CrossRef](#)]
14. Aucelli, P.P.C.; Fortini, P.; Roszkopf, C.M.; Scorpio, V.; Viscosi, V. Recent channel adjustments and riparian vegetation response: Some examples from Molise (Italy). *Geogr. Fis. Dinam. Quat.* **2011**, *34*, 161–173. [[CrossRef](#)]
15. Crowell, M.; Leatherman, S.P.; Buckley, M.K. Shoreline Change Rate Analysis: Long Term versus Short Term Data. *Shore Beach* **1993**, *61*, 13–20.
16. US Army Corps of Engineers. *Shore Protection Manual*; Coastal Engineering Research Centre: Washington, DC, USA, 1984.
17. Buccino, M.; Tuozzo, S.; Ciccaglione, M.C.; Calabrese, M. Predicting Crenulate Bay Profiles from Wave Fronts: Numerical Experiments and Empirical Formulae. *Geosciences* **2021**, *11*, 208. [[CrossRef](#)]
18. Ashton, A.D.; Murray, A.B. High-angle wave instability and emergent shoreline shapes: 1. Modeling of sand waves, flying spits, and capes. *J. Geophys. Res.* **2006**, *111*, F04011. [[CrossRef](#)]
19. Ashton, A.D.; Murray, A.B. High-angle wave instability and emergent shoreline shapes: 2. Wave climate analysis and comparisons to nature. *J. Geophys. Res.* **2006**, *111*, F04012. [[CrossRef](#)]
20. Pelnard-Considere, R. Essai de theorie de l’evolution des formes de rivages en plage de sable et de galets. In *4th Journees de l’Hydraulique, Les Energies De La Mer*; Question III, Rapport No. 1; Société Hydrotechnique de France: Paris, France, 1956; pp. 289–298.
21. Hallermeier, W.A. Field Data on Seaward Limit of Profile Change. *J. Waterw. Port. Coast.* **1985**, *111*, 598–602.
22. Hasselmann, K.; Dunkel, M.; Ewing, J.A. Directional wave spectra observed JONSWAP. *J. Phys. Oceanogr.* **1973**, *10*, 1264–1280. [[CrossRef](#)]
23. Contini, P.; De Girolamo, P. Impatto Morfologico di Opere a Mare: Casi di studio. In Proceedings of the VIII Conference Italian Association Offshore and Marina, La Spezia, Italy, 28–29 May 1998.
24. Holthuijsen, L.H. *Waves in Oceanic and Coastal Waters*; University of Cambridge Press: Cambridge, UK, 2007.
25. Buccino, M.; del Vita, I.; Calabrese, M. Predicting wave transmission past Reef Ball™ submerged breakwaters. *J. Coast. Res.* **2013**, *SI 65*, 171–176. [[CrossRef](#)]
26. N.W.H.; Bruce, T.; De Rouck, J.; Kortenhuis, A.; Pullen, T.; Schüttrumpf, H.; Troch, P.; Zanuttigh, B. 2018. Available online: [www.overtopping-manual.com](http://www.overtopping-manual.com) (accessed on 1 November 2018).
27. Buccino, M.; Daliri, M.; Dentale, F.; Di Leo, A.; Calabrese, M. CFD experiments on a low crested sloping top caisson breakwater. Part 1. Nature of loadings and global stability. *Ocean. Eng.* **2019**, *182*, 259–282. [[CrossRef](#)]
28. Buccino, M.; Daliri, M.; Dentale, Calabrese, M. CFD experiments on a low crested sloping top caisson breakwater. Part 2. Analysis of plume impact. *Ocean. Eng.* **2019**, *182*, 345–357. [[CrossRef](#)]
29. Hamm, L.; Peronnard, C. Wave parameters in the nearshore: A clarification. *Coast. Eng.* **1997**, *32*, 119–135. [[CrossRef](#)]